

## THE MAGNETIC FIELD TOWARD THE YOUNG PLANETARY NEBULA K 3-35

Y. GÓMEZ, AND D. TAFOYA<sup>1</sup>

Centro de Radioastronomía y Astrofísica, UNAM, Apartado Postal 3-72, Morelia, Michoacán 58089, Mexico.

G. ANGLADA AND L. F. MIRANDA

Instituto de Astrofísica de Andalucía, CSIC, Apdo. Correos 3004, E-18080 Granada, Spain

J. M. TORRELLES

Instituto de Ciencias del Espacio (CSIC)-IEEC, Facultat de Física, Universitat de Barcelona, Planta 7a, Martí i Franquès 1, 08028 Barcelona, Spain

N. A. PATEL

Center for Astrophysics, 60 Garden Street, Cambridge, MA 02138, USA

AND

R. FRANCO HERNÁNDEZ<sup>1</sup>

Centro de Radioastronomía y Astrofísica, UNAM, Apartado Postal 3-72, Morelia, Michoacán 58089, Mexico.

*Draft version November 13, 2018*

### ABSTRACT

K 3-35 is a planetary nebula (PN) where H<sub>2</sub>O maser emission has been detected, suggesting that it departed from the proto-PNe phase only some decades ago. Interferometric VLA observations of the OH 18 cm transitions in K 3-35 are presented. OH maser emission is detected in all four ground state lines (1612, 1665, 1667, and 1720 MHz). All the masers appear blueshifted with respect to the systemic velocity of the nebula and they have different spatial and kinematic distributions. The OH 1665 and 1720 MHz masers appear spatially coincident with the core of the nebula, while the OH 1612 and 1667 MHz ones exhibit a more extended distribution. We suggest that the 1665 and 1720 masers arise from a region close to the central star, possibly in a torus, while the 1612 and 1667 lines originate mainly from the extended northern lobe of the outflow. It is worth noting that the location and velocity of the OH 1720 MHz maser emission are very similar to those of the H<sub>2</sub>O masers (coinciding within 0<sup>''</sup>.1 and  $\sim 2$  km s<sup>-1</sup>, respectively). We suggest that the pumping mechanism in the H<sub>2</sub>O masers could be produced by the same shock that is exciting the OH 1720 MHz transition. A high degree of circular polarization (>50%) was found to be present in some features of the 1612, 1665, and 1720 MHz emission. For the 1665 MHz transition at  $\sim +18$  km s<sup>-1</sup> the emission with left and right circular polarizations (LCP and RCP) coincide spatially within a region of  $\sim 0$ ''<sup>0</sup>.3 in diameter. Assuming that these RCP and LCP 1665 features come from a Zeeman pair, we estimate a magnetic field of  $\sim 0.9$  mG within 150 AU from the 1.3 cm continuum peak. This value is in agreement with a solar-type magnetic field associated with evolved stars.

*Subject headings:* ISM: planetary nebulae: individual(K 3-35) — masers — polarization - magnetic fields

### 1. INTRODUCTION

K 3-35 (PN G056.0+0.20; IRAS 19255+2123) is an extremely young PN where we are observing the first stages of formation of collimated bipolar outflows (Miranda et al. 1998). Its radio continuum emission at 3.6 cm exhibits an elongated, filamentary S-shape with a remarkable point-symmetric structure with respect to the center (Aaquist 1993; Miranda et al. 2001; Gómez et al. 2003). Recently, its morphology has been successfully modeled with a precessing jet evolving in a dense asymptotic giant branch (AGB) circumstellar

medium (Velázquez et al. 2007). The extension of the radio continuum jets at 3.6 cm is  $\sim 2$ '' , which is equivalent to 10,000 AU (assuming a distance of 5 kpc; Zhang 1995). A short dynamical age (<50 years) for the jets was estimated from Velázquez et al. (2007), which is comparable with that of the core. In addition, the high ratio of molecular to ionized mass (Tafoya et al. 2007) indicates that K 3-35 departed from the proto-PN phase only some decades ago.

K 3-35 was the first PN known to exhibit H<sub>2</sub>O maser emission (Miranda et al. 2001). Since then, two other PNe have been reported with H<sub>2</sub>O maser emission: IRAS 17347–3139 (de Gregorio-Monsalvo et al. 2004) and IRAS 18061–2505 (Gómez et al. 2008). The water masers toward K 3-35 are located at the center of the nebula, along the minor axis, at a radius of  $\sim 85$  AU and also at the tips of the jet lobes (Miranda et al. 2001).

Electronic address: y.gomez@astrosmo.unam.mx, d.tafoya@astrosmo.unam.mx

Electronic address: guillem@iaa.es, lfm@iaa.es

Electronic address: torrelles@ieec.fcr.es

Electronic address: npatel@cfa.harvard.edu

Electronic address: r.franco@astrosmo.unam.mx

<sup>1</sup> Predoctoral Student at the Center for Astrophysics, 60 Garden Street, Cambridge, MA 02138, USA

Uscanga et al. (2008) have analyzed the kinematics of the H<sub>2</sub>O masers in K 3-35, identifying the presence of a rotating and expanding ring with a radius of  $\sim 100$  AU, which may be related with the collimation of the outflow.

The mechanism that generates collimated outflows in PNe and their role in the shaping of these objects is still a matter of debate. Magnetic fields have been suggested to play a major role in these aspects; their existence in circumstellar envelopes has been invoked to explain jets and bipolar morphologies in PNe (e.g. Rozyczka & Franco 1996; García-Segura et al. 1999; García-Segura 2006; Matt et al. 2000, 2004; Blackman et al. 2001; García-Segura et al. 2005; Frank et al. 2007). García-Segura & López (2000) have modeled morphologies of PNe with and without magnetic fields, showing the importance of magnetic fields to produce collimated ejections. Soker (2006) has argued that the magnetic fields in PNe cannot shape the morphology of the nebula alone without the presence of a stellar companion that produces a spin-up mechanism in the envelope. The detection of magnetized disks toward evolved stars is therefore crucial to understand the generation of collimated jets and bipolar structures in PNe.

Magnetic fields have been detected in several proto-PNe (Zijlstra et al. 1989; Kemball & Diamond 1997; Vlemmings et al. 2005, 2006; Bains et al. 2003; Etoka & Diamond 2004; Szymczak & Gérard 2005; Herpin et al. 2006; Vlemmings & van Langevelde 2008) but only toward a few PNe (Miranda et al. 2001; Greaves 2002; Jordan et al. 2005). The strength of the magnetic fields detected in envelopes of evolved objects ranges from 1 G, at a radius of  $r \sim 1$  AU, to  $10^{-4}$  G, at  $r \sim 1000$  AU, and is of the order of kG in the central stars of PNe (Jordan et al. 2005). Recently, the geometry of the magnetic field has been inferred for the proto-PN W43A (Vlemmings et al. 2005) and the PNe NGC 7027, NGC 6537, and NGC 6302 (Greaves 2002; Sabin et al. 2007) suggesting the presence of toroidal magnetic fields. In the particular case of K 3-35, it shows polarized OH maser emission in the 1665 MHz line around the central region, with a high level of circular polarization above  $\simeq 50\%$ , suggesting the presence of a magnetic field (Miranda et al. 2001; Gómez et al. 2005).

In this work we present VLA<sup>2</sup> observations toward K 3-35 of the OH maser emission in its four ground-state transitions (1612, 1665, 1667 and 1720 MHz) in order to study the spatial distribution and polarization of the masers as well as the magnetic field in this PN.

## 2. OBSERVATIONS

The OH maser observations towards K 3-35 at 1612.231, 1665.401, 1667.359 and 1720.530 MHz were carried out on 2002 March 31 with the VLA. The array was in the A configuration giving an angular resolution of  $\sim 1''$  at 18 cm. The 1665 and 1667 OH main lines were observed with a total bandwidth of 195.31 kHz, divided into 256 channels of 0.763 kHz each. The velocity resolution for these transitions was  $\sim 0.14$  km s<sup>-1</sup> covering a total velocity range of 35 km s<sup>-1</sup>. The 1612 and 1720

OH satellite lines were observed with a total bandwidth of 781.25 kHz, divided into 256 channels of 3.05 kHz each, achieving a velocity resolution of  $\sim 0.56$  km s<sup>-1</sup> yielding a total velocity range of  $\sim 140$  km s<sup>-1</sup>.

The calibration, deconvolution, and imaging of the data were carried out using the Astronomical Image Processing System (AIPS) of the NRAO. Both the right circular polarization (RCP) and the left circular polarization (LCP) were observed simultaneously using the normal spectral line mode centered at a  $v_{LSR} = +15$  km s<sup>-1</sup> for all transitions, except the 1667 MHz line which was centered at  $+4$  km s<sup>-1</sup>. We applied Hanning smoothing to all four OH transitions in order to improve the signal-to-noise ratio of the data, and to minimize the Gibbs phenomenon. The resulting *rms* per channel is  $\sim 6$  mJy beam<sup>-1</sup> for the 1665, 1667, and 1720 MHz transitions and  $\sim 30$  mJy beam<sup>-1</sup> for the 1612 MHz transition. The *rms* for the 1612 MHz transition is higher due to strong on-line flagging and a shorter integration time. The absolute amplitude calibrator was 1331+305, the phase calibrator 1925+211, and the bandpass calibrator 0319+415. The flux densities of these calibrators for each frequency are summarized in Table 1. The RCP and LCP data were calibrated separately and later combined during the imaging process to make Stokes I = (I<sub>RCP</sub> + I<sub>LCP</sub>)/2 and Stokes V = (I<sub>RCP</sub> - I<sub>LCP</sub>)/2 data sets, where I<sub>RCP</sub> and I<sub>LCP</sub> are the intensities in the right and left circular polarizations, respectively. Cleaned images for the RCP and LCP data were made using the task IMAGR of AIPS with the ROBUST parameter (Briggs 1995) set to 0, allowing to determine the peak position of the OH masers, at each velocity channel, with a relative accuracy of  $\sim 0''.05$ .

## 3. RESULTS AND DISCUSSION

### 3.1. Continuum and OH Maser Emissions

Figure 1 shows the 18 cm continuum emission toward K 3-35, taken from the line-free channels of the OH spectral data. The continuum emission has a deconvolved angular size of  $1''.8 \times 0''.5$ , P.A. =  $16^\circ$ . This 18-cm continuum image shows a northeast-southwest elongation which resemble the orientation of the bipolar outflow (Aaquist 1993; Miranda et al. 2001). The total continuum flux density at 18 cm is  $18 \pm 1$  mJy with a peak position at  $\alpha(2000) = 19^h 27^m 44.^s 026 \pm 0.^s 001$ ,  $\delta(2000) = 21^\circ 30' 03''.57 \pm 0''.04$ .

The 18 cm nominal peak position is located toward the north, about  $\sim 0''.13$ , of the 1.3 cm peak position reported by Miranda et al. (2001). We attribute this shift in position to the fact that the 18 cm emission might be optically thick, while the 1.3 cm is optically thin, then the 1.3 cm peak may appear closer to the central star than the 18 cm peak. However, since the uncertainty in the absolute position for the 18 cm data is about  $0''.1$ , observations with higher absolute positional accuracy are needed to confirm this spatial shift.

The OH 1665 and 1667 MHz main lines, as well as the OH 1612 and 1720 MHz satellite lines were all detected and imaged toward K 3-35. Figure 2 shows the RCP, LCP, I and V spectra made with the task ISPEC of AIPS, for the four ground-state lines. The detected OH maser emission lines appear with LSR velocities  $< 23$  km s<sup>-1</sup>, which are all blueshifted with respect to the systemic velocity of the source derived from the CO (2-1) molecu-

<sup>2</sup> The Very Large Array (VLA) is operated by the National Radio Astronomy Observatory (NRAO), facility of the National Science Foundation operated under cooperative agreement by Associated Universities, Inc.

lar gas ( $\sim 23 \text{ km s}^{-1}$ ; Tafuya et al. 2007). In general, the OH maser spectrum in an evolved star is characterized by two peaks which are blueshifted and redshifted, coming mainly from the front and back parts of the expanding envelope, respectively (Reid et al. 1977). In the presence of an ionized region, which is the case for K 3-35, and since the ionized gas can become optically thick at low frequencies, it is possible that the redshifted maser components, coming from the back side of the nebula, are not detected because the emission could be absorbed by the free-free opacity of the ionized gas (Rodríguez et al. 1985). This effect may explain why in K 3-35 all the OH masers are blueshifted with respect to the systemic velocity.

In Table 2 we list the velocity, position, and flux density of the observed features in the OH RCP and LCP 1665, 1667, 1612 and 1720 MHz spectra (see Figure 2). We define a maser feature as all the spectral channels in which maser emission is detected, indicated by the properties of its peak channel. Also, we define a maser spot as one spectral channel of a maser feature. The velocities and spatial distribution of the OH maser spots are shown in Figure 3. The positions were obtained by 2D Gaussian fitting in each velocity channel where the OH maser emission was above  $5\text{-}\sigma$  level, with a typical uncertainty of  $0''.05$  (see Table 2). Only one single maser component was fitted per channel and in all cases it is spatially unresolved ( $\leq 1''$ ).

It can be noticed from Figure 3, that the masers for the different transitions are located toward different regions of the nebula. In particular, the OH 1665 and 1720 masers have a compact distribution, around the 1.3 cm continuum emission peak, compared with the 1612 and 1667 masers that appear in a more extended area (see Figure 3). On the other hand, the OH 1665 and 1667 MHz masers are tracing different kinematic components, with the 1667 maser spots having velocities lower than  $10 \text{ km s}^{-1}$ . In what follows, we present an analysis of the spatial distribution, kinematics and polarization for each individual OH maser transition.

### 3.1.1. 1665 MHz

Engels et al. (1985) did not detect the OH 1665 MHz transition toward K 3-35 with a  $3\text{-}\sigma$  sensitivity limit of 0.6 Jy. Miranda et al. (2001) detected and imaged for the first time the 1665 MHz transition toward K 3-35 using the VLA, reporting the presence of emission in a velocity range from  $+14$  to  $+20 \text{ km s}^{-1}$ . In this work (Figure 2 and Table 2) we confirm the presence of OH 1665 MHz maser emission, which covers the same LSR velocity range as reported by Miranda et al. (2001). The velocity, position, and flux density of the OH 1665 MHz RCP and LCP spectral features are listed on Table 2. The location of the OH 1665 maser spots (with signal-to-noise ratios  $> 5$ ), appear slightly shifted to the south of the 18 cm radio continuum peak (see Figure 3). Almost all these maser spots fall within  $0''.1$  of the position of the 1.3 cm radio continuum peak, which we think is closer to the central star. Also, almost all the OH 1665 MHz features exhibit a high degree of circular polarization above 50% and, in the particular case of the spectral feature in the velocity range from  $+17.5$  to  $+18.0 \text{ km s}^{-1}$ , the RCP and LCP emission is spatially coincident, suggesting the

presence of a Zeeman pair.

### 3.1.2. 1667 MHz

Two weak 1667 MHz spectral components toward K 3-35 were first reported by Engels et al. (1985) at LSR velocities of  $-4$  and  $+7.8 \text{ km s}^{-1}$ , and intensities of 0.3 and 0.4 Jy, respectively. te Lintel Hekkert (1991) did not detect the OH 1667 MHz masers with an upper limit of 0.2 Jy. Miranda et al. (2001) reported the detection of 1667 MHz maser emission in two velocity ranges, from  $-2$  to  $-3 \text{ km s}^{-1}$  and from  $+7$  to  $+9 \text{ km s}^{-1}$ , with peak flux densities lower than 0.1 Jy. In this work we report the detection of two 1667 MHz spectral features at  $-3.5$  and  $+8.0 \text{ km s}^{-1}$  (see Figures 2, 3, and Table 2), that are spatially separated in two groups by about  $0''.1$ , toward the northeast and the southwest, respectively (see blue and green features in Figure 3). There is no significant circular polarization in the OH 1667 MHz masers ( $\leq 16\%$ ; see Table 2) in agreement with the results of Miranda et al. (2001). The two features are blueshifted with respect to the systemic velocity of the PN ( $\sim +23 \text{ km s}^{-1}$ ), suggesting that they are arising from the blueshifted lobe of the outflow. In any case, it is clear from Figure 3, that the 1667 maser emission is tracing a different region than the 1665 one.

### 3.1.3. 1612 MHz

The OH 1612 MHz line was first detected toward K 3-35 by Engels et al. (1985) using the Effelsberg 100 m telescope. Three velocity features (at  $-4$ ,  $+9$  and  $+20 \text{ km s}^{-1}$ ) were reported, with the strongest feature ( $\sim 4 \text{ Jy}$ ) at  $+9 \text{ km s}^{-1}$ . te Lintel Hekkert (1991), using the Nançay radio telescope, observed two 1612 MHz velocity features at  $\sim +9$  and  $+20 \text{ km s}^{-1}$ . High spectral resolution 1612 MHz observations, carried out also with the Nançay radio telescope by Szymczak & Gérard (2004), showed the presence of four velocity features (at  $-2$ ,  $+9$ ,  $+18$  and  $+21 \text{ km s}^{-1}$ ). Interferometric VLA observations revealed the coincidence in position (within  $\sim 0''.5$ ) of the 1612 MHz maser emission and the continuum emission peak, supporting the association of the OH masers with K 3-35 (Aaquist 1993). In this work we confirm that the OH 1612 maser emission is associated with K 3-35 (Figure 3). Four OH 1612 maser spectral features were detected at  $-2.0$ ,  $+8.8$ ,  $+18.4$  and  $+21.2 \text{ km s}^{-1}$  (Figure 2 and Table 2), in agreement with those reported by Szymczak & Gérard (2004). We note that the OH 1612 maser spots are displaced in position by about  $0''.1$  to the south of the 1.3 cm continuum peak and that they show an extended distribution in space (see Figure 3).

In Figure 2 we identify four main groups of 1612 MHz maser features. Two of them coincide in velocity with those of the 1667 MHz transition at  $\sim -3.5$  and  $+8 \text{ km s}^{-1}$ , although only the group at  $+8 \text{ km s}^{-1}$  coincides spatially with that of the 1667 MHz transition (see green color maser spots in Figure 3), suggesting that both the OH 1612 and 1667 velocity transitions are arising in the same region, (i.e. in the northern blueshifted lobe of the outflow) (Miranda et al. 2000). The third and fourth groups of OH 1612 MHz masers at  $\sim +18$  and  $+21 \text{ km s}^{-1}$  appear in the same velocity range as the 1665 transition, and it is more likely that they are arising from an inner region of the nebula, close to the central star. All the features show circular polarization, with

the highest polarized feature at  $+21 \text{ km s}^{-1}$  (orange red color spots in Figure 3).

### 3.1.4. 1720 MHz

The OH 1720 MHz maser emission has been detected previously toward K 3-35 by te Lintel Hekkert (1991) when the classification of this object was still unclear. Now it is known that K 3-35 is a young PN (Miranda et al. 2001) and so far it is the only one that exhibits the OH 1720 MHz maser transition. te Lintel Hekkert (1991) detected a single peak spectral component toward K 3-35 centered at  $+22.1 \text{ km s}^{-1}$  with a total flux density of 3 Jy. Our 1720 MHz detection (see Figure 2) shows a narrow velocity feature centered at an LSR velocity of  $+21.4 \text{ km s}^{-1}$  (0.6 Jy), coincident in position with the radio continuum peak at 1.3 cm (red color maser spots in Figure 3), suggesting that these masers originate very close to the central star.

The OH 1720 MHz maser emission is commonly associated with shocked molecular regions in star forming regions and supernovae remnants (Frail et al. 1994). Recently, the 1720 MHz transition has been detected toward a few post-AGB stars (Sevenster & Chapman 2001; Deacon et al. 2004). Elitzur (1976) has proposed that the only way to produce strong OH 1720 MHz maser emission is by means of collisional pumping under particular physical conditions ( $T_k \leq 200 \text{ K}$ ;  $n_{\text{H}_2} \simeq 10^5 \text{ cm}^{-3}$ ). Sevenster & Chapman (2001) detected OH 1720 MHz maser emission toward the post-AGB star IRAS 18043–2116, and explained this emission as due to the passage of a C-type shock through the remnant AGB envelope caused by the fastwind. According to the scenario proposed by these authors,  $\text{H}_2\text{O}$  molecules would be formed behind the shock. Subsequently, the  $\text{H}_2\text{O}$  is photodissociated enhancing the OH abundance. The post-shock physical conditions are favorable for pumping the OH 1720 MHz maser transition. Even though these authors predicted that  $\text{H}_2\text{O}$  masers would not be present, Deacon et al. (2004) detected  $\text{H}_2\text{O}$  maser emission toward IRAS 18043–2116. These results suggest that the physical conditions in this source can be adequate to excite both the OH 1720 MHz and the  $\text{H}_2\text{O}$  maser emissions.

For K 3-35 we note that the velocity and location of the OH 1720 MHz masers are very similar to those of the  $\text{H}_2\text{O}$  masers within  $0''.1$ , which correspond to the absolute positional accuracy for the OH masers. This suggest that the pumping mechanism of the  $\text{H}_2\text{O}$  masers could be produced by the same shock that is exciting the OH 1720 MHz transition. The OH 1720 MHz maser emission has a high degree of circular polarization,  $\sim 50\%$  (Table 2); however, although the RCP and LCP maser features coincide in position (within  $0''.04$ ), they do not show the typical ‘‘S’’ profile, indicative of a Zeeman pattern in the Stokes parameter V.

### 3.2. Magnetic field in K 3-35

Polarization studies have been carried out toward proto-PNe using OH maser transitions (e.g. Bains et al. 2003; Szymczak & Gérard 2004),  $\text{H}_2\text{O}$  masers (Vlemmings et al. 2005; Vlemmings & van Langevelde 2008) and SiO masers (Herpin et al. 2006), showing for some objects magnetic field components which are

orthogonal to the major axis of the nebulae. Several PNe have been reported to harbor OH maser emission (Payne et al. 1988; Zijlstra et al. 1989; Bowers & Knapp 1989; te Lintel Hekkert & Chapman 1996). However, the relatively weakness of the OH maser features difficults the detection of polarization using OH maser techniques. In the case of K 3-35, the OH maser emission is strong enough to allow us a detailed study of the polarization of this emission.

The existence of strong circular polarization in some features of the OH 1612, 1665 and 1720 MHz maser transitions suggests the presence of a magnetic field in K 3-35. In general, the field leads to a splitting of the magnetic substates of the OH molecule, which can be detected as a Zeeman pair (Davies 1974; Crutcher & Kazes 1983). Assuming that the source is permeated with the same strength of field then, if a Zeeman effect is present, the LCP and RCP components have to be emitted from the same region of the OH source.

Figure 4 shows a close up of the RCP and LCP 1665 MHz maser spots plotted in Figure 3 (upper left panel) but with maser spots that have flux densities above  $15\sigma$ . These maser spots are mainly distributed in three spatial regions with different characteristic velocities: one close to the 1.3 cm continuum emission peak (marked with the upper dash-line square in Figure 4) and the other two located toward the southeast (left dash-line square) and southwest (right dash-line circle) of the 1.3 cm continuum peak. The region associated with the 1.3 cm continuum peak corresponds to the main spectral feature, at  $\sim +17.1 \text{ km s}^{-1}$  of the RCP spectrum shown in Figure 2 (upper left panel). The two regions to the southeast and southwest are separated in position by about  $0''.04$ , and correspond to the two spectral features at  $\sim +15.0$  and  $+18.6 \text{ km s}^{-1}$ , respectively, of the LCP spectrum shown in Figure 2 (upper left panel). The relative position accuracy between the LCP 1665 masers is less than  $0''.006$ , and the resulting velocity resolution (after Hanning smoothing) is  $\sim 0.3 \text{ km s}^{-1}$ , then we consider that this positional and velocity shift is real. The shift between these two groups of OH 1665 features may be simply due to inhomogeneities of the gas at different velocities or they can reveal a true kinematic effect of a single structure. If we try to extrapolate the kinematics of the ring traced by the  $\text{H}_2\text{O}$  masers (Uscanga et al. 2008), we note that the sense of rotation for the  $\text{H}_2\text{O}$  ring is not in agreement with the velocity gradient of the two OH 1665 MHz groups (see bottom left panel of Figure 4). We suggest that only the group of masers around  $+18.6 \text{ km s}^{-1}$  could be associated with dense gas close to the central star, likely in an equatorial torus, but the OH 1665 masers at  $\sim +15 \text{ km s}^{-1}$ , would be associated with the blueshifted lobe of the outflow as in the case of the 1667 and 1612 MHz masers.

We also note that the positions of the 1665 RCP and LCP maser spots with velocities  $\sim +17.5$  to  $+18.0 \text{ km s}^{-1}$ , overlap each other (see dash-line circle in upper-left panel of Figure 4). In this sense, the OH 1665 transition has a velocity component that seems to follow the physical requirements for a Zeeman pattern (they exhibit the typical ‘‘S’’ shape in the Stokes V spectrum shown in Figure 2). Assuming that these masers are arising from the same spatial region (within  $0''.03$ ) and that we have at least one Zeeman pair in the velocity range between

+17.5 to +18.0 km s<sup>-1</sup>, we can estimate the magnitude of the magnetic field along the line-of-sight ( $B_{LOS}$ ).

It is known that when the Zeeman splitting is small compared to the line width, the Stokes V spectrum is given by  $V = dI/d\nu b B_{LOS} \text{ Hz } \mu\text{G}^{-1}$  (Heiles et al. 1993; Robishaw et al. 2008), where  $dI/d\nu$  is the frequency derivative of the Stokes I spectrum and  $b$  is the splitting coefficient ( $b=3.270$  for the OH 1665 MHz transition; Davies 1974). In terms of the velocity, the previous expression will be  $V = 3.27 c/\nu_0 dI/d\nu B_{LOS} \text{ Hz } \mu\text{G}^{-1}$ , where  $c=3\times 10^5 \text{ km s}^{-1}$  and  $\nu_0=1665\times 10^6 \text{ Hz}$ . By comparing the Stokes V spectrum with the derivative of the Stokes I spectrum, we obtain  $V=0.55 \text{ km s}^{-1} dI/d\nu$ . From this scaling, we estimate  $B_{LOS} \simeq 0.9 \pm 0.1 \text{ mG}$ , at a distance, from the 1.3 cm continuum peak, of  $\sim 0''.03$  ( $\sim 150 \text{ AU}$ ).

A comparison between the magnetic field estimates toward evolved stars as function of distance from the star, assuming a  $B \propto r^\alpha$  dependence, has been made by Vlemmings et al. (2005), plotting two models: a solar-type magnetic field ( $\alpha=-2$ ), and a dipole magnetic field ( $\alpha=-3$ ). Plotting the strength of the magnetic field of K 3-35 in figure 6 of Vlemmings et al. (2005), shows that it is in agreement with a solar-type model.

#### 4. CONCLUSIONS

Using the VLA we detected and imaged the 1612, 1665, 1667 and 1720 MHz OH masers toward K 3-35. The velocity and position distribution of the masers suggest that they are arising from different regions in the nebula. The 1665 and 1720 MHz maser features have a compact distribution, near the 1.3 cm continuum emission peak, and it is possible that some features of the 1665 MHz transition are originating in an equatorial disk. The 1612 and 1667 MHz maser features are spread in a more ex-

tended region in two main velocity groups. We suggest that the velocity component at  $\sim +8.0 \text{ km s}^{-1}$  in the 1612 and 1667 MHz spectra could be tracing the same region near the central core in the blueshifted lobe of the outflow. As far as we know, K 3-35 is the only PN that exhibits simultaneously OH 1720 MHz and H<sub>2</sub>O maser emission. We note that the velocity and location of the OH 1720 MHz masers are very similar to those of the H<sub>2</sub>O masers. This suggests that the pumping mechanism of the H<sub>2</sub>O masers could be produced by the same shock that is exciting the OH 1720 MHz transition. The 1612, 1665, and 1720 MHz spectra show some velocity features with a high degree of circular polarization ( $>50\%$ ). In the particular case of the velocity feature at  $\sim +18 \text{ km s}^{-1}$  in the OH 1665 MHz transition, it shows the typical ‘‘S’’ profile for the Stokes V, and the LCP and RCP features are arising from the same spatial position (within  $\sim 0''.03$  in diameter). This result suggests that a Zeeman pair could be present in K 3-35 and a magnetic field in the line-of-sight of  $\sim 0.9 \text{ mG}$ , at a radius of 150 AU, is estimated. This value is in agreement with a solar-type ( $\alpha=-2$ ,  $B \propto r^\alpha$ ) magnetic field associated with evolved stars.

YG, DT and RFH acknowledge support from DGAPA, UNAM, and CONACYT, Mexico. GA and JMT acknowledge support from MEC (Spain) AYA 2005-08523-C03 and MICINN (Spain) AYA 2008-06189-C03 grants (co-funded with FEDER funds). LFM is supported partially by grant AYA2005-01495 of the Spanish MEC and grant AYA2008-01934 of the Spanish MICINN (both co-funded by FEDER funds). GA, LFM, and JMT acknowledge partial support from Junta de Andalucía (Spain).

#### REFERENCES

- Aaquist, O., 1993, *A&A*, 267, 260  
 Bains, I., Gledhill, T., Yates, J. & Richards, A. 2003, *MNRAS*, 338, 287  
 Blackman, E.G., Frank, A., Markiel, J.M., Thomas, J.H., Van Horn, H.M. 2001, *Nature*, 409, 485  
 Bowers, P. F. & Knapp, G. R. 1989, *ApJ*, 347, 325  
 Briggs, D. S. 1995, Ph.D. thesis, New Mexico Inst. Mining Technology  
 Crutcher, R. M. & Kazes, I. 1983, *A&A*, 125, 23  
 Davies, R. D. 1974, in *IAU Symp. 60, Galactic Radio Astronomy*, ed. F. J. Kerr & S. C. Simonson, III (Dordrecht: Reidel), 275  
 Deacon, R. M., Chapman, J. M. & Green, A. J. 2004, *ApJS*, 155, 595  
 de Gregorio-Monsalvo, I., Gómez, Y., Anglada, G., Cesaroni, R., Miranda, M., Gómez, J. F., & José M. Torrelles, 2004, *ApJ*, 601, 921.  
 Elitzur, M. 1976, *A&A*, 52, 213  
 Engels, D., Schmid-Burgk, J., Walmsley, C.M. & Winnberg, A. 1985, *A&A*, 148, 344  
 Etoka, S., & Diamond, P. 2004, *MNRAS*, 348, 34  
 Frail, D. A., Goss, W. M., Slysh, V. I. 1994, *ApJ*, 424, 111  
 Frank, A., De Marco, O., Blackman, E., & Balick, B. 2007, [arXiv:0712.2004]  
 García-Segura, G., Langer, N., Rozyczka, M., & Franco, J. 1999, *ApJ*, 489, L189  
 García-Segura, G. & López, J. A. 2000, *ApJ*, 544, 336  
 García-Segura, G., López, J. A., & Franco, J., 2005, *ApJ*, 618, 919  
 García-Segura, G. 2006, *IAU 243, Planetary Nebulae in our Galaxy and Beyond*. Edited by Michael J. Barlow and Roberto H. Méndez. Cambridge: Cambridge University Press, p.297  
 Gómez, Y., Miranda, L. F., Anglada, G., & Torrelles, J. M. 2003, in *IAU 209, Planetary Nebulae*, (Sn Francisco:ASP), p.263  
 Gómez, Y., Tafoya, D., Anglada, G., Franco-Hernández, R., Torrelles, J. M., Miranda, L. F., 2005, *MmSAI*, 76, 472  
 Gómez, J. F., Suárez, O., Gómez, Y., Miranda, L. F., Torrelles, J. M., Anglada, G. & Morata, O. 2008, *AJ*, 135, 2074  
 Greaves, J. S. 2002, *A&A*, 392, 1  
 Heiles, C., Goodman, A. A., McKee, C. F. & Zweibel, E. G., 1993, in *Protostars and Planets III*, ed. E. H. Levy & J. I. Lunine (Tucson: Univ. Arizona Press), 279  
 Herpin, F., Baudry, A., Thum, C., Morris, D. & Wiesemeyer, H., 2006, *A&A*, 450, 667  
 Jordan, S., Werner, K. & O’Toole, S. J. 2005, *A&A*, 432, 273  
 Kembell, A. J. & Diamond, P. J. 1997, *ApJ*, 481, L111  
 Matt, S., Balick, B., Winglee, R. & Goodson, A., 2000, *ApJ*, 545, 965  
 Matt, S., Frank, A., & Blackman, E. G. 2004, in *ASP Conf. Ser. 313, Asymmetric Planetary Nebulae III*, ed. M. Meixner et al. (San Francisco: ASP), 449.  
 Miranda, L. F., Fernández, M., Alcalá, J. M., Guerrero, M. A., Anglada, G., Gómez, Y., Torrelles, J. M. & Aaquist, O. B. 2000, *MNRAS*, 311, 748  
 Miranda, L. F., Gómez, Y., Anglada, G. & Torrelles, J. M. 2001, *Nature*, 414, 284.  
 Miranda, L. F., Torrelles, J. M., Guerrero, M. A., Aaquist, O. B., & Eiroa, C., 1998, *MNRAS*, 298, 243.  
 Payne, H. E., Phillips, J. A. & Terzian, Y. 1988, *ApJ*, 326, 368  
 Reid, M. J., Muhleman, D. O., Moran, J. M., Johnston, K. J., & Schwartz, P. R. 1977, *ApJ*, 214, 60  
 Robishaw, T., Quataert, E. & Heiles, C. 2008, *ApJ*, 680, 981  
 Rodríguez, L. F., Gómez, Y. & García-Barreto, J. A. 1985, *RMxAA*, 11, 109  
 Rozyczka, M. & Franco, J. 1996, *ApJ*, 469, L127  
 Sabin, L., Zijlstra, A. A. & Greaves, J. S., 2007, *MNRAS*, 376, 378

- Sevenster, M. N. & Chapman, J. M. 2001, *ApJ*, 546, L119
- Soker, N. 2006, *PASP*, 118, 260
- Sun, J. & Kwok, S. 1987, *A&A*, 185, 258
- Szymczak, M. & Gérard, E. 2004, *A&A*, 423, 209
- Szymczak, M. & Gérard, E. 2005, *A&A*, 433, L29
- Tafoya, D., Gómez, Y., Anglada, G., Loinard, L., Torrelles, J. M., Miranda, L. F., Osorio, M., Franco-Hernández, R., Nyman, L.-A., Nakashima, J. & Deguchi, S. 2007, *AJ*, 133, 364
- te Lintel Hekkert, P., 1991, *A&A*, 248, 209
- te Lintel Hekkert, P. & Chapman, J. M., *A&AS*, 1996, 119, 459
- Uscanga, L., Gómez, Y., Raga, A. C., Cantó, J., Anglada, G., Gómez, J. F., Torrelles, J. M. & Miranda, L. F., 2008, *MNRAS*, 390, 1127
- Velázquez, P. F., Gómez, Y., Esquivel, A. & Raga, A. C. 2007, *MNRAS*, 382, 1965
- Vlemmings, W. H. T., van Lagevelde, H. J. & Diamond, P. J. 2005, *A&A*, 434, 1029
- Vlemmings, W. H. T., Diamond, P. J. & Imai, H. 2006, *Nature*, 440, 58
- Vlemmings, W. H. T. & van Langevelde, H. J., 2008, *A&A* 488, 619
- Zijlstra, A. A., Te Lintel Hekkert, P., Pottasch, S. R., Caswell, J. L., Ratag, M. & Habing, H. J. 1989, *A&A*, 217, 157
- Zhang, C. Y. 1995, *ApJSS*, 98, 659

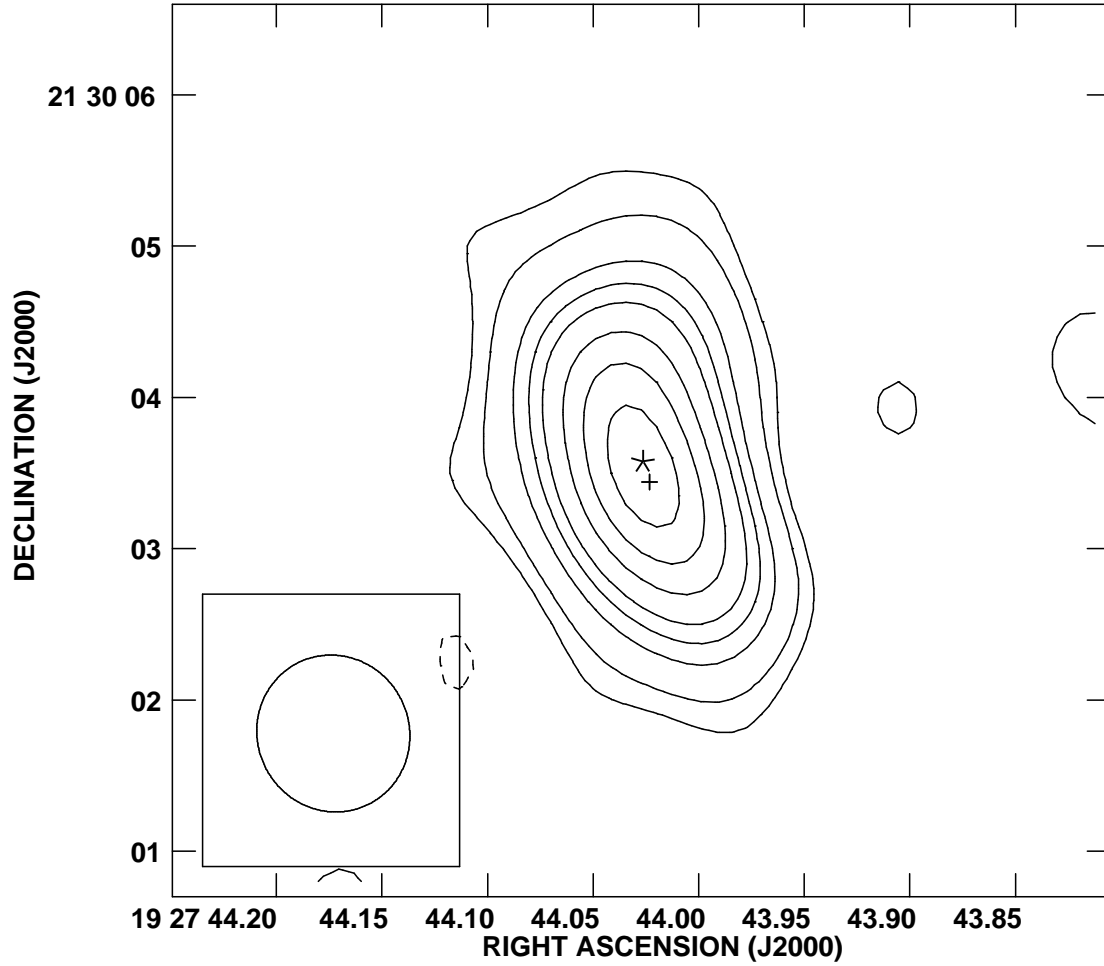


FIG. 1.— VLA 18 cm continuum contour image of K 3-35 (beam size is  $\sim 1''$ , shown in the bottom left corner of the image). The contours are  $-3, 3, 5, 7, 9, 12, 15, 20,$  and  $30$  times  $0.3 \text{ mJy beam}^{-1}$ , the *rms* noise of the image. The cross marks the continuum peak position at  $1.3 \text{ cm}$  at  $\alpha(2000) = 19^{\text{h}} 27^{\text{m}} 44^{\text{s}} 0233$ ,  $\delta(2000) = 21^{\circ} 30' 03'' 441$ , (Miranda et al. 2001; Uscanga et al. 2008). The star marks the peak position of the  $18 \text{ cm}$  continuum at  $\alpha(2000) = 19^{\text{h}} 27^{\text{m}} 44^{\text{s}} 026$ ,  $\delta(2000) = 21^{\circ} 30' 03'' 57$  (this work). Note the NE-SW elongation of the emission that follows the same orientation as the bipolar outflow reported at higher frequencies (Miranda et al. 2001).

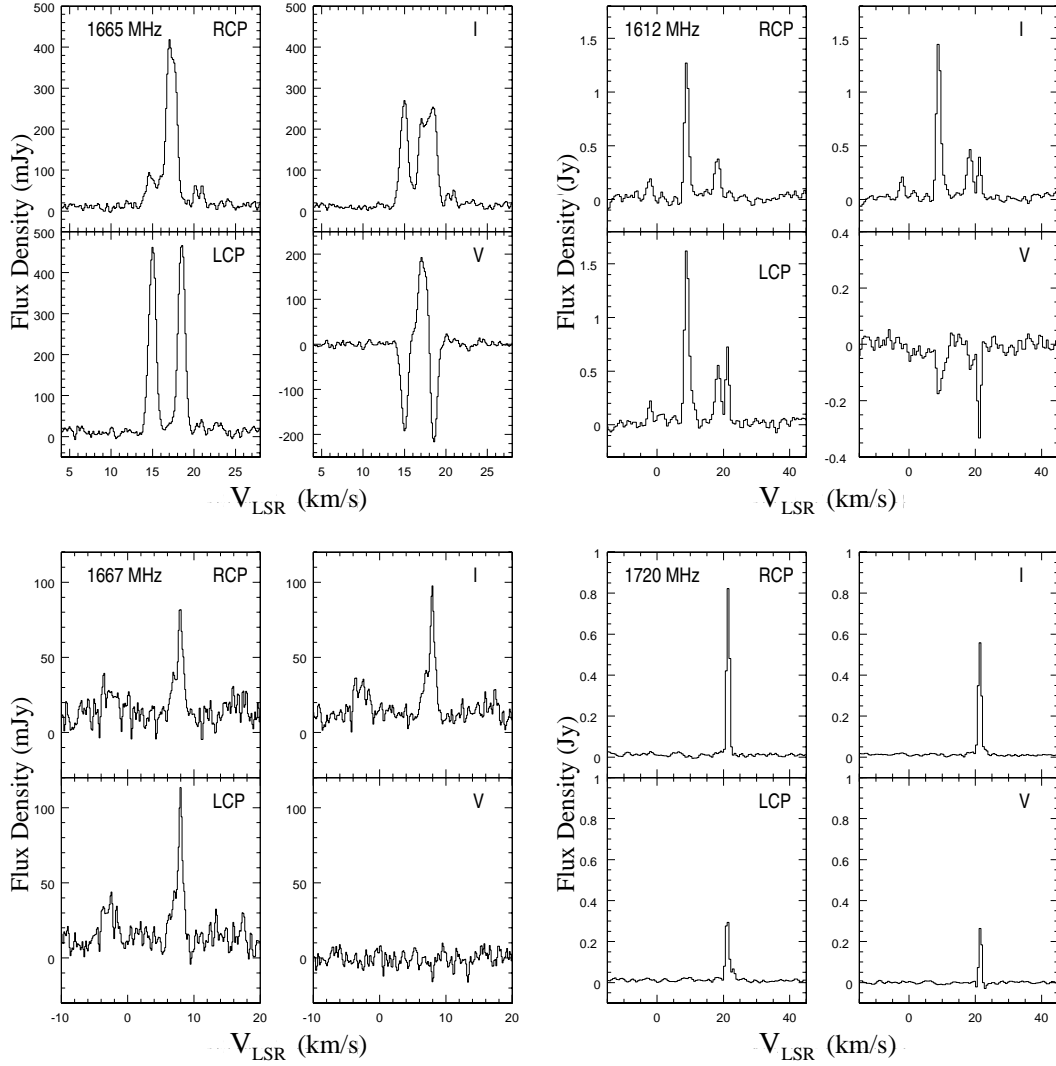


FIG. 2.— RCP, LCP, I and V spectra toward K 3-35, for the 1665, 1667, 1612, and 1720 MHz OH transitions. The spectra were obtained by integrating the emission in a box of  $5'' \times 5''$  centered on the continuum emission peak at 18 cm. The systemic  $V_{LSR}$  velocity of the source is  $\sim 23$  km s $^{-1}$ . Note the “S” profile in the Stokes parameter V in the 1665 MHz transition at  $\sim 18$  km s $^{-1}$ , indicating a Zeeman pattern.

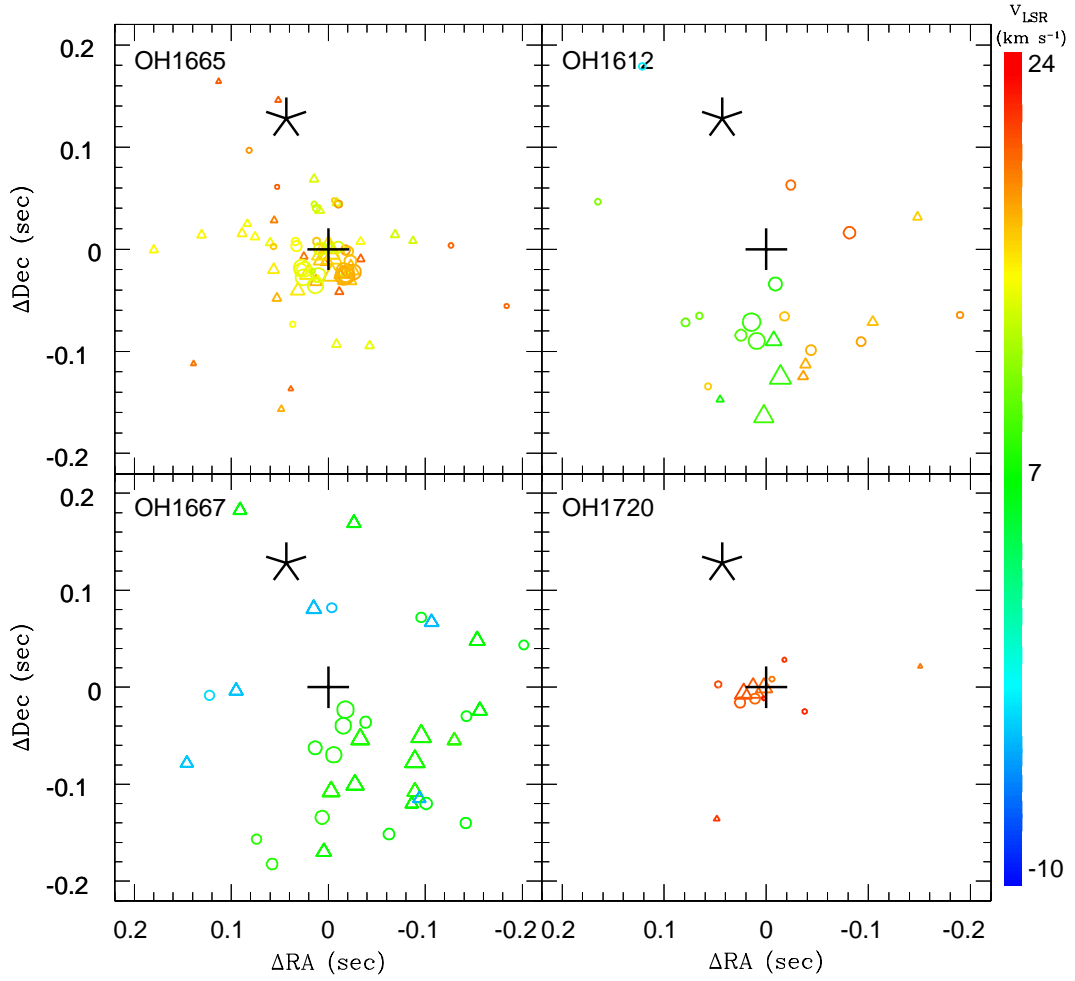


FIG. 3.— OH maser spots for the 1665, 1667, 1612 and 1720 MHz transitions toward the young PN K 3-35. The circles mark the left circular polarization (LCP) and the triangles the right circular polarization (RCP). Only maser spots with signal-to-noise ratio  $>5$  were plotted. The maser spots have been plotted with the same color-coded velocity that is shown at the right side. The linear size of the symbols is proportional to the square root of the integrated flux density. The black cross (0,0) marks the continuum peak position at 1.3 cm and the black star marks the peak position of the 18 cm continuum (see §3.1).

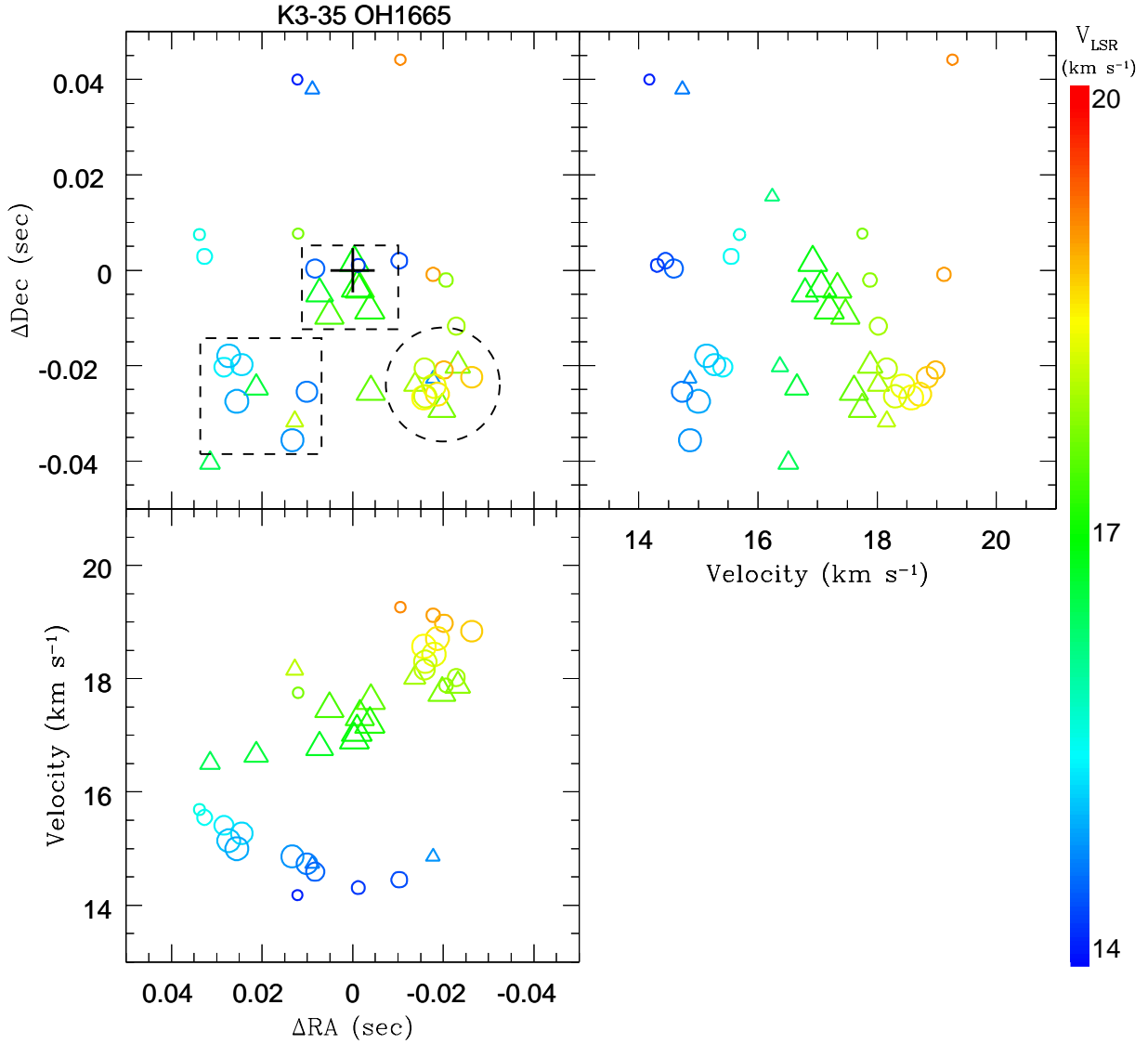


FIG. 4.— Close-up of the position-velocity diagrams for the 1665 MHz transition along the declination (top-right panel) and right ascension (bottom-left panel) of K 3-35. Only maser spots above  $15\sigma$  were plotted, in order to note the three different groups that have been marked with two black dash-line squares and one black dash-line circle. The OH maser spots have been plot with the same color-coded velocity. The color circles mark the left circular polarization (LCP) and the triangles the right circular polarization (RCP) spots. The black dash-line circle marks the region where we suggest there is a Zeeman pair (see §3.2). The black cross indicates the 1.3 cm peak continuum position.

TABLE 1  
CALIBRATOR FLUX DENSITIES

Frequency (MHz)	Flux Density (Jy)		
	Amplitude 1331+305 <sup>a</sup>	Phase 1925+211 <sup>b</sup>	Bandpass 0319+415 <sup>b</sup>
1665	13.631	1.094±0.005	23.1±0.1
1667	13.623	1.087±0.005	23.4±0.1
1612	13.852	1.216±0.027	... <sup>c</sup>
1720	13.412	1.069±0.007	23.4±0.3

<sup>a</sup> Adopted flux density.

<sup>b</sup> Bootstrapped flux density for the phase and bandpass calibrators, respectively.

<sup>c</sup> The bandpass calibrator was not observed at 1612 MHz.

TABLE 2  
OH MASER SPECTRAL FEATURES OBSERVED TOWARD K 3-35<sup>a</sup>

Transition MHz	RCP					LCP					m <sub>c</sub> <sup>e</sup> (%)
	V <sub>LSR</sub> <sup>b</sup> (km s <sup>-1</sup> )	S <sub>ν</sub> (mJy)	α(J2000) <sup>c</sup> (s)	δ(J2000) <sup>c</sup> (")	Δ <sup>d</sup> (")	V <sub>LSR</sub> <sup>b</sup> (km s <sup>-1</sup> )	S <sub>ν</sub> (mJy)	α(J2000) <sup>c</sup> (s)	δ(J2000) <sup>c</sup> (")	Δ <sup>d</sup> (")	
1665	21.0	61.6	44.020	03.40	0.04	21.0	42.4	44.020	03.40	0.05	+18
	20.1	66.1	44.020	03.40	0.06	20.1	14.6	43.991	03.60	0.10	+64
	18.6	37.0	44.020	03.30	0.10	18.6	482.0	44.0200	03.400	0.005	-86
	17.1	422.6	44.0200	03.400	0.007	17.1	36.5	44.027	03.60	0.15	+84
	15.0	82.1	44.020	03.40	0.04	15.0	474.8	44.0271	03.400	0.006	-71
	14.6	99.8	44.027	03.40	0.04	14.6	304.7	44.020	03.40	0.01	-51
1667	8.0	87.8	44.020	03.40	0.04	8.0	114.3	44.020	03.40	0.03	-13
	-3.5	43.0	44.027	03.60	0.07	-3.5	33.8	44.020	03.60	0.09	+12
1612	21.2	<90 <sup>f</sup>	...	...	...	21.2	774.3	44.018	03.46	0.02	-90
	18.4	383.2	44.021	03.33	0.06	18.4	578.6	44.020	03.34	0.04	-20
	8.8	1496.6	44.022	03.31	0.01	8.8	1815.8	44.024	03.37	0.01	-10
	-2.0	155.8	44.039	03.76	0.16	-2.0	261.6	44.032	03.62	0.08	-25
1720	21.4	838.7	44.0242	03.437	0.003	21.4	306.5	44.0251	03.425	0.007	+47

<sup>a</sup> A maser feature is defined as all the spectral channels in which maser emission is detected, indicated by the properties of its peak channel.

<sup>b</sup> Central velocity of the channel.

<sup>c</sup> Position obtained by a Gaussian fitting of the emission in each channel (α(2000)= 19<sup>h</sup> 27<sup>m</sup> ... , δ(2000)= 21° 30' ... ).

<sup>d</sup> Relative positional error

<sup>e</sup> m<sub>c</sub> Percentage of circular polarization (100×V/I)

<sup>f</sup> 3σ upper limit